

Enhanced giant magnetoresistance in Ni-doped antiperovskite compounds $\text{GaMn}_{3-x}\text{Ni}_x$ ($x=0.05, 0.10$)

B. S. Wang,¹ P. Tong,^{1,a)} Y. P. Sun,^{1,2,b)} L. J. Li,¹ W. Tang,¹ W. J. Lu,¹ X. B. Zhu,¹ Z. R. Yang,¹ and W. H. Song¹

¹Key Laboratory of Materials Physics, Institute of Solid State Physics, Hefei 230031, People's Republic of China

²High Magnetic Field Laboratory, Chinese Academy of Sciences, Hefei 230031, People's Republic of China

(Received 2 October 2009; accepted 6 November 2009; published online 3 December 2009)

We report an enhanced negative giant magnetoresistance (GMR) with larger temperature span in Ni-doped antiperovskite compounds $\text{GaMn}_{3-x}\text{Ni}_x$. The observed GMR can peak at $\sim 75\%$ (at 85 kOe) and exceed 60% (at 50 kOe) over a temperature span of approximate 110 and 50K for $x=0.05$ and 0.10, respectively. Compared with the parent GaMn_3 , the well-enhanced GMR in Ni-doped samples is suggested to be associated with the partially suppressed antiferromagnetic (AFM) ground state, which favors the transition from the high-resistivity AFM state to the low-resistivity canted ferromagnetic state under an external magnetic field. © 2009 American Institute of Physics. [doi:10.1063/1.3268786]

Recently, the Mn-based antiperovskite compounds AXMn_3 (A: main group elements; X: carbon or nitrogen) have attracted considerable attention due to their interesting properties, such as giant magnetoresistance (GMR),¹ magnetocaloric effect (MCE),²⁻⁴ giant negative thermal expansion,⁵⁻⁸ and magnetostriction effect.⁹ As a typical antiperovskite-structured compound, GaMn_3 has been intensively investigated in the past decades.^{1-3,10-12} With decreasing temperature, three phase transitions were observed: one second-order transition from paramagnetic to ferromagnetic (FM) phase at 246 K, the other second-order transition from FM to intermediate canted ferromagnetic (CFM) exists around 160 K; a first-order transition from the CFM state to antiferromagnetic (AFM) ground state with a discontinuous lattice expansion in volume at 158 K.^{1-3,10,11} A plateaulike temperature dependence of GMR has been observed with the maximum MR value of 50% at 50 kOe, covering a temperature range of about 20 K.^{1,11} It has been proved that the GMR is associated with the field-induced magnetic transition from AFM phase to CFM phase or FM phase (FM and CFM are undistinguishable by magnetization measurements) where a close correlation among lattice, spin, and charge exists.¹¹ However, few reports have been focused on optimization of the GMR effect in GaMn_3 such as enhancing the peak values of MR, broadening the temperature span, and reducing the critical magnetic fields. In this letter, we report an obviously enhanced GMR in Ni-doped $\text{GaMn}_{3-x}\text{Ni}_x$. For $x=0.05(0.10)$, the MR exceeds 60% (70%) at 50 kOe, covering a temperature range of about 110 K (50 K). For both samples, the maximum MR values are approaching 75% under a magnetic field of 85 kOe. The essential mechanism is discussed in terms of field-induced magnetic transition and the electronic characteristic of Ni-substitution.

Polycrystalline $\text{GaMn}_{3-x}\text{Ni}_x$ ($0 \leq x \leq 0.10$) were prepared by direct reaction of the constituent elements of Ga (4N), Graphite (3N), Mn (4N), and Ni (4N).²⁻⁴ The x-ray

diffraction patterns collected at room temperature and the Rietveld refinements confirm that the samples are good in quality with $x \leq 0.10$. The lattice shrinks in the doped samples, e.g., the volume of $x=0.05$ shrinks by $\Delta V/V_0 = -0.323\%$ compared with GaMn_3 . Further increasing the level of doping, impurities appear in the final samples. Samples with $x=0.05$ and 0.10 were subjected to further measurements. The magnetization measurements were performed on a quantum design superconducting quantum interference device magnetometer ($1.8 \text{ K} \leq T \leq 400 \text{ K}$, $0 \leq H \leq 50 \text{ kOe}$). The resistivity was measured using the standard four-probe technique in a quantum design physical property measurement system ($1.8 \text{ K} \leq T \leq 400 \text{ K}$, $0 \leq H \leq 90 \text{ kOe}$).

Figure 1 illustrates the temperature dependence of electrical resistivity (ρ) and MR [defined as $\text{MR} = (\rho_H - \rho_0) / \rho_0$] for $x=0.05, 0.10$ measured at various magnetic fields. As

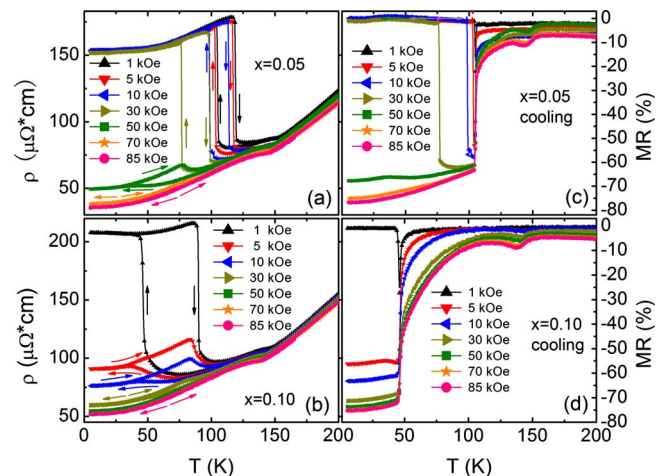


FIG. 1. (Color online) Temperature dependence of electrical resistivity at various magnetic fields up to 85 kOe in both cooling and warming processes: (a) $x=0.05$ and (b) $x=0.10$. The temperature dependence of MR at various magnetic fields calculated from the results of [(a) and (b)]; (c) $x=0.05$; and (d) $x=0.10$. The arrows indicate the direction of temperature circle.

^{a)} Author to whom correspondence should be addressed. Electronic mail: tongpeng@issp.ac.cn. Tel.: +86-551-559-2757. FAX: +86-551-559-1434.

^{b)} Electronic mail: ypsun@issp.ac.cn.

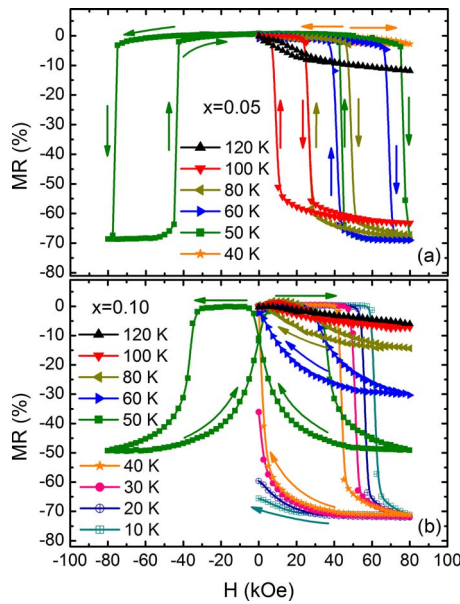


FIG. 2. (Color online) Variation in MR vs magnetic field at several selected temperatures in increasing and decreasing field processes: (a) $x=0.05$ and (b) $x=0.10$. The arrows indicate the directions of field variation.

shown in Figs. 1(a) and 1(b), the $\rho(T)$ shows a metallic behavior in both AFM and FM phases, and an abrupt change of the resistivity occurs accompanying the AFM-CFM transition (T_{AC}), which can be ascribed to the sharp change of carriers concentration as described in GaCMn_3 .¹ Another feature is that the sharp change in $\rho(T)$ at zero field can be completely suppressed in decreasing/increasing temperature cycles with a critical field of 50 and 5 kOe for $x=0.05$ and 0.10, respectively, resulting in a large MR with a large temperature span. Meanwhile, these values of critical magnetic field are much lower than that of the parent GaCMn_3 (more than 240 kOe),¹ indicating a weaker AFM ground state in Ni-doped samples. Figures 1(c) and 1(d) presents the MR as function of temperature for both samples. For $x=0.05$, the MR at 50 kOe (30 kOe) can exceed 65% (60%) over a temperature of approximate 110 K (32 K) when samples were cooled from the room temperature. Analogously, for $x=0.10$ MR at 50 kOe (5 kOe) exceeds 70% (56%) with a temperature span of 50 K (45 K). For both cases, the plateaulike MR increases with increasing magnetic fields, reaching 75% at 85 kOe.

Figure 2 shows the field dependence of MR at several selected temperatures below T_{AC} with the magnetic field up to 85 kOe. For $x=0.05$, in a wide range from 50 to 100 K, the MR exceeds 60% and the largest MR values at 50 and 60 K exceed 70%. Further, at 100 K, a completely recoverable saturated MR of 65% can be achieved in a magnetic field of 40 kOe. At 120 K, the MR recovered only a value of 15% because the sample is situated in stable CFM or FM phase. In the case of 40 K or lower temperatures, the MR values are very small. However, as shown in Fig. 1(c), the MR can approach 80% at 40 K in an external field of 85 kOe. This behavior is related to sample's magnetization history and will be discussed in the following text. As to $x=0.10$, when the temperature is lower than 40 K, the MR shows a sharp increase at a certain critical field which increases as decreasing temperature. Meanwhile, in the process of demagnetization, the peak value of MR ($>70\%$) can be obtained at a

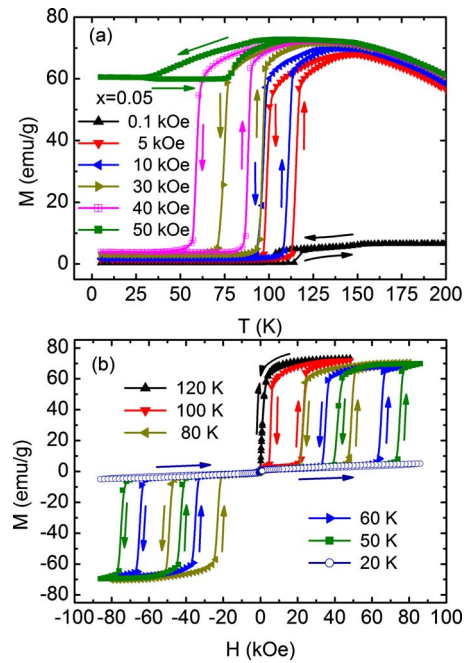


FIG. 3. (Color online) (a) Temperature dependence of magnetization $M(T)$ for the sample $x=0.05$ in cooling and warming processes at various fields up to 50 kOe. The arrows indicate the direction of temperature circle. (b) Isotherm magnetization curves $M(H)$ of the sample with $x=0.05$ at selected temperatures and the arrows indicate the directions of field variation.

small magnetic field, the origin of which can be attributed to weak AFM interaction in sample with $x=0.10$. Above 40 K, the MR is basically recovery at 80 kOe though the peak value of MR reduces as the temperature increases.

Figure 3(a) shows the temperature dependence of magnetization $M(T)$ for $x=0.05$ measured at different magnetic fields. Obviously, an abrupt change in $M(T)$ around T_{AC} can be observed. Meanwhile, the value of T_{AC} was reduced with increasing the magnetic field. When the external magnetic field exceeds 50 kOe, the $M(T)$ was remarkably enhanced at low temperatures. The results are in good agreement with the field dependence of MR and ρ (shown in Fig. 1), implying that there exist close correlations between electronic transport and magnetic properties. Figure 3(b) displays the isotherm magnetization $M(H)$ of $x=0.05$ at various temperatures. Between 50 and 120 K (below T_{AC} at zero field), $M(H)$ shows a metamagnetic transition, triggered by the external magnetic field, from the low-magnetization AFM to the high-magnetization FM phase with a magnetization change of 70 emu/g. Above 120 K, the curves exhibit FM behavior, corresponding to the small MR values ($<20\%$) as shown in Fig. 2(a). The $M(H)$ at 20 K exhibits AFM behavior without sharp changes up to 85 kOe. However, as displayed in Fig. 3(a), the transition from low-magnetization AFM to high-magnetization CFM state can be observed even when the field is larger than 50 kOe. This difference and that of low-temperature MR values between $MR(T)$ and $MR(H)$ as mentioned above can be interpreted by considering its magnetization history. For $M(T)$ [Fig. 3(a)] and $\rho(T)$ [Fig. 1(a)] or $MR(T)$ [Fig. 1(c)], the sample was cooled down with the measurement magnetic fields turned on from the room temperature. It is beneficial to the nucleation and growth of FM domains at low temperatures, accordingly to the field-induced AFM-CFM transition. However, for $M(H)$ [Fig.

3(b)] and $MR(H)$ [Fig. 2(a)], the sample was cooled down from the room temperature to the measurement temperatures with zero magnetic field. Therefore, it is relatively hard to induce the AFM-CFM transition at low temperatures even if the external field is as large as 85 kOe. For $x=0.10$, the AFM ground state is further suppressed so that the AFM-CFM transition can be triggered at 10 K even if the sample was cooled without magnetic field [to see Fig. 2(b)].

As discussed above, the GMR observed here is closely related to the field-induced AFM-CFM (or FM) transition. In the parent $GaCMn_3$, the ground AFM state is somewhat robust so that a high magnetic field of 240 kOe is required to suppress the AFM ground state.¹ The measurement of Hall effect reveals that the average carrier density (electron-type) in the FM (CFM) phase is about five times larger than that in the AFM phase.¹ Further, the substitution of Ni for Mn in $GaCMn_3$ can be seen as electron-type doping, favoring the FM state and weakening the AFM ground state.^{1,4} Consequently, the slight Ni-doping weakens the AFM ground state and favors the field-induced AFM-FM transition, leading to the enhanced MR.

Generally speaking, the shrink of lattice favors the FM interaction among Mn sites, as observed in current system. Similarly, as reported recently in $GaN(Mn_{1-x}Fe_x)_3$, the AFM ground state was gradually suppressed by Fe doping and a FM ground state appears when $x \geq 0.05$, while the lattice constant decreases.¹³ However, there are few exceptions, such as $GaN_{1-x}C_xMn_3$, in which C doping induces FM state and expands the lattice at the same time.¹⁴ This discrepancy indicates the relation between lattice constant and magnetic coupling among Mn sites in doped Mn-based antiperovskite $AXMn_3$ is more complex than simply thought. Compared with average structural information, local lattice distortion may be more useful to a better understanding of unique properties in element-substituted $AXMn_3$.⁶

The enhanced MR effect in the Ni-doped samples is comparable with those observed recently in other three-dimensional (3D) GMR systems, such as FM shape memory alloys $Ni_{50}Mn_{50-x}In_x$ ($x=14-16$) (MR $\sim 70\%$ at 50 kOe),¹⁵ Heusler alloys $Ni_{41}Co_9Mn_{39}Sb_{11}$ (MR $\sim 70\%$ at 100 kOe),¹⁶ $Ni_{50}Mn_{36}Sn_{14}$ (MR $\sim 50\%$ at 170 kOe),¹⁷ and $Mn_2Sb_{1-x}Sn_x$ ($0 < x \leq 0.4$) (60% at 50 kOe).¹⁸ For practical applications, it is necessary to control or reduce the thermal hysteresis associated with the first-order transition. In spite of this, the enhanced MR with lower operation magnetic field makes the Ni-doped samples more applicable than the parent one. The hysteresis of rich fine structure in $M(H)$ curves [to see Fig. 3(b)] evidences the reverse transition by the applied magnetic fields, suggesting its potential application as a magnetic switch in the corresponding temperature range.¹⁹ In fact, in the Mn-based antiperovskite compounds $AXMn_3$, magnetic phase transitions accompanied by abrupt changes of magnetization, resistivity, and lattice have been widely observed, which is thought to be related to the reconstruction of electronic structure.^{1,4-8,11} In comparison with

A-site doping, the effect of Mn-sites doping has been less extensively studied. Since the Fermi surface mainly originates from 3D electrons,¹² these two kinds of doping methods may influence the physical properties in different ways. From this point of view, Mn-site doping can be an effective way for exploring large MCE and GMR properties, as well as for understanding the unique coupling among lattice, spin, and charges.

In summary, the obviously enhanced GMR effect, which is associated with field-induced AFM-CFM transition, was observed in $GaCMn_{3-x}Ni_x$ ($x=0.05$ and 0.10). The observed MR has a saturated value of $\sim 75\%$ (at 85 kOe) and is larger than 60% (at 50 kOe), covering a large temperature span. The enhanced MR in $GaCMn_{3-x}Ni_x$ can be attributed to the weakened AFM ground state by Ni-doping, which favors the field-induced magnetic transition. It is suggested that substitution of other 3D elements for Mn provides an effective way to adjust their physical properties, e.g., MR effect, as has been demonstrated in this letter.

This work was supported by the National Key Basic Research under Contract No. 2007CB925002, and the National Natural Science Foundation of China under Contract Nos. 50701042, 10774146, and 10974205 and Director's Fund of Hefei Institutes of Physical Science, Chinese Academy of Sciences.

¹K. Kamishima, T. Goto, H. Nakagawa, N. Miura, M. Ohashi, N. Mori, T. Sasaki, and T. Kanomata, *Phys. Rev. B* **63**, 024426 (2000).

²T. Tohei, H. Wada, and T. Kanomata, *J. Appl. Phys.* **94**, 1800 (2003).

³M. H. Yu, L. H. Lewis, and A. R. Moodenbaugh, *J. Appl. Phys.* **93**, 10128 (2003).

⁴B. S. Wang, P. Tong, Y. P. Sun, X. Luo, X. B. Zhu, S. B. Zhang, X. D. Zhu, Z. R. Yang, J. M. Dai, and W. H. Song, *Europhys. Lett.* **85**, 47004 (2009).

⁵K. Takenaka, K. Asano, M. Misawa, and H. Takagi, *Appl. Phys. Lett.* **92**, 011927 (2008).

⁶S. Iikubo, K. Kodama, K. Takenaka, H. Takagi, M. Takigawa, and S. Shamoto, *Phys. Rev. Lett.* **101**, 205901 (2008).

⁷R. J. Huang, L. F. Li, F. S. Cai, X. D. Xu, and L. H. Qian, *Appl. Phys. Lett.* **93**, 081902 (2008).

⁸K. Takenaka and H. Takagi, *Appl. Phys. Lett.* **94**, 131904 (2009).

⁹K. Asano, K. Koyama, and K. Takenaka, *Appl. Phys. Lett.* **92**, 161909 (2008).

¹⁰D. Fruchart, E. F. Bertaut, F. Sayetat, M. N. Eddine, R. Fruchart, and J. P. Senateur, *Solid State Commun.* **8**, 91 (1970).

¹¹W. S. Kim, E. O. Chi, J. C. Kim, H. S. Choi, and N. H. Hur, *Solid State Commun.* **119**, 507 (2001).

¹²K. Motizuki and H. Nagai, *J. Phys. C* **21**, 5251 (1988).

¹³K. Takenaka, T. Inagaki, and H. Takagi, *Appl. Phys. Lett.* **95**, 132508 (2009).

¹⁴Ph. l'Heritier, D. Boursier, R. Fruchart, and D. Fruchart, *Mater. Res. Bull.* **14**, 1203 (1979).

¹⁵S. Y. Yu, Z. H. Liu, G. D. Liu, J. L. Chen, Z. X. Cao, G. H. Wu, B. Zhang, and X. X. Zhang, *Appl. Phys. Lett.* **89**, 162503 (2006).

¹⁶S. Y. Yu, M. Liu, G. D. Liu, Z. H. Liu, J. L. Chen, Z. X. Cao, G. H. Wu, B. Zhang, and X. X. Zhang, *Appl. Phys. Lett.* **90**, 242501 (2007).

¹⁷K. Koyama, H. Okada, K. Watanabe, T. Kanomata, R. Kainuma, W. Ito, K. Oikawa, and K. Ishida, *Appl. Phys. Lett.* **89**, 182510 (2006).

¹⁸Y. Q. Zhang and Z. D. Zhang, *Phys. Rev. B* **67**, 132405 (2003).

¹⁹R. Waser and M. Aono, *Nature Mater.* **6**, 833 (2007).